

Full length article

Effects of notches on the deformation behavior of submicron sized metallic glasses: Insights from *in situ* experimentsR. Lakshmi Narayan^{a,b}, Lin Tian^b, Danli Zhang^b, Ming Dao^{c,***}, Zhi-Wei Shan^{b,**}, K. Jimmy Hsia^{d,*}^a Department of Materials Science and Engineering, Carnegie Mellon University, Pittsburgh, PA 15213, USA^b Center for Advancing Materials Performance from the Nanoscale (CAMP-Nano), Hysitron Applied Research Center in China (HARCC), State Key Laboratory for Mechanical Behavior of Materials, Xi'an Jiaotong University, Xi'an, Shaanxi 710049, PR China^c Department of Materials Science and Engineering, Massachusetts Institute of Technology, 77 Massachusetts Avenue, Cambridge, MA 02139, USA^d Department of Mechanical Engineering and Department of Biomedical Engineering, Carnegie Mellon University, Pittsburgh, PA 15213, USA

ARTICLE INFO

Article history:

Received 7 March 2018

Received in revised form

15 May 2018

Accepted 17 May 2018

Available online 19 May 2018

Keywords:

Metallic glass

Notch sensitivity

Strength

Ductility

Nano mechanical test

In situ TEM

ABSTRACT

Reducing the size of metallic glasses (MG) to submicron or nanoscale levels improves their strength and ductility. However, there is no clear consensus in the literature regarding their mechanical behavior in the presence of a flaw or notch. In this work, quantitative tensile tests on notched submicron sized CuZr MG specimens were conducted inside a transmission electron microscope to study their deformation characteristics. Strength was found to be notch insensitive for shallow notched thick specimens, although reducing specimen dimensions and increasing notch sharpness enhances it by 14%. It was reasoned that the severity with which shear bands are geometrically constrained determines the strength and fracture morphology of notched specimens. Softening, accompanied with a transition to necking failure, occurs when the width of ligament that connects the notches is smaller than 80 nm. The competition between shear band propagation and plastic zone growth-mediated homogeneous activation of shear transformation zones was found to be responsible for this brittle to ductile transition. Current results provide unique insights into the various design aspects to be considered for reliable engineering of small scale components.

© 2018 Acta Materialia Inc. Published by Elsevier Ltd. All rights reserved.

1. Introduction

Metallic glasses (MGs), in addition to possessing an impressive suite of mechanical properties like high strength, resilience and wear resistance [1], are easily processable [2–6], which makes them ideal materials for designing miniaturized components with intricate shapes in nano electromechanical (NEMS) devices [3,6]. A concomitant feature of designing intricate shapes is that the fabricated components, accidentally or intentionally, contain notches, incisions and sharp corners. These artifacts locally elevate or concentrate stresses when the component is mechanically loaded. Therefore, the applicability of MGs in NEMS devices will

critically depend on their mechanical behavior, more specifically their strength and plasticity, in the presence of notches.

It has been observed that the *notch sensitivity* of strength, for most engineering materials, is a function of length scale. For instance, the tensile strength of bulk sized crystalline components is highly notch sensitive, wherein they become weaker in the presence of notches [7,8]. However, when the component dimension is reduced to the nanoscale, the strength and toughness become insensitive to notches or flaws [9–14]. This contrasting behavior has been attributed to the differences in the way plasticity, mediated by dislocations or grain re-alignments, interacts with the internal microstructures (e.g., grain boundaries and twins) and external geometry (sample dimensions), respectively, at the two extreme length scales [13,15,16]. In the case of MGs, a clear consensus on the notch sensitivity of tensile strength and plasticity has not yet been established at these extreme length scales. While experiments and simulations on bulk alloys by Kimura and Masumoto [17], Wang et al. [18] and Pan et al. [19] encourage the notion of increased nominal strength with increasing notch sharpness,

* Corresponding author.

** Corresponding author.

*** Corresponding author.

E-mail addresses: mingdao@mit.edu (M. Dao), zwshan@xjtu.edu.cn (Z.-W. Shan), kjhsia@cmu.edu (K.J. Hsia).

similar experiments by Flores and Dauskardt [20] indicate an inverse correlation between the two. Furthermore, Qu et al. [21,22] assert that MGs are notch insensitive materials. At the submicron and nano scales, molecular dynamics (MD) [23] and continuum simulations [24,25] predict higher strength and ductility of notched tensile MG specimens compared to their unnotched counterparts. Conversely, experiments conducted by Gu et al. [26] suggest that the strength and ductility of MG specimens decrease in the presence of notches.

One reason for this lack of consensus regarding notch sensitivity of MGs, compared to the well-established trends in crystalline materials, is the obscurity associated with the structure and deformation mechanisms in the former. In crystalline materials, owing to atomic periodicity, defects like dislocations, twins and interfaces can be easily identified as the principal flow units of deformation with well-defined characteristic length scales. However, in MGs, isolating flow units is a non-trivial process as its atoms are arranged non-periodically and the microstructure has no distinguishable features. Therefore, although theories and models involving shearing of loosely packed atomic clusters, also known as shear transformation zones (STZs) [27], have been developed, it is difficult to isolate or characterize them directly. Furthermore, the strains in MGs localize rapidly during deformation and the STZs develop into shear bands (SBs). To understand the notch sensitivity of deformation from the perspective of STZs, free volume and SB dynamics poses a unique challenge. This challenge is amplified by the lack of systematic experimental investigations at the nano scale, which is nevertheless difficult to perform in the first place. In this work, we conduct notched tensile experiments, on a Cu-Zr MG, inside a transmission electron microscope (TEM) using a quantitative mechanical testing system. The specimen dimensions and notch aspect ratios are systematically varied to examine subtle changes in strength and plasticity. By incorporating key features of the existing deformation models, the results are then analyzed and compared with predictions in literature.

2. Experimental methods

A melt spun Cu₄₉Zr₅₁ MG was used in this study. Free-standing, double notched tensile plate specimens were fabricated using focused ion beam (FIB, FEI Nanolab 600). The final FIB trim and notch cut were performed using the ultra-mild milling conditions of 16 kV and ~1.5 pA. Since milling with the Ga ion beam can induce structural changes, which in turn can also potentially influence the mechanical behavior of the material, the composition of the specimens at different points was determined using energy dispersive X-ray spectroscopy (EDX) in the TEM. The Ga content in each specimen did not exceed 1%, suggesting that the milling conditions would have negligible influence on the results of this study. To further eliminate the effects of FIB induced damage, a nano mill (M1040, Fischione) was employed as a final step to slightly thin the specimen. Thickness and cross section area of the gauge section for each specimen was measured after fracture using a scanning electron microscope (SEM). For more details on preparing free standing tensile specimens, refer to Tian et al. [28,29]. The uniaxial tensile tests were carried out using the quantitative capability of a Hysitron PI95 TEM PicoIndenter. The tests were performed under displacement control mode at a nominal strain rate of 1×10^{-3} /s. The test specimen was gripped and aligned inside a JEOL 2100F TEM operating at 200 kV. Owing to the non-trivial nature of designing and performing these experiments, only up to 3 tests could be repeated for each specimen condition.

Since the electron beam can generate heat and potentially influence the results of the mechanical tests, imaging, inside the TEM, was performed at an e-beam current density of 2×10^{-2} A cm⁻².

Previous tests on the same material, with similar dimensions as used in this paper, have confirmed that the deformation characteristics are unaffected by the e-beam, at or below this current density [28,29]. In addition, since a large heat-conducting tungsten grip is in intimate contact with the small specimen, heating effects would be negligible. All the tests were recorded by a charge-coupled device camera (Gatan 833 CCD), placed inside the TEM, operating at a capture rate of 10 frames/s.

After conducting the tensile tests the fractured cross-section of each specimen was viewed inside the high resolution SEM. This was primarily done to measure the dimensions (thickness and width) of the unnotched ligament in each specimen. Note that since the length of all the ligaments are of the order of 20–150 nm, variations in their thicknesses are assumed to be negligible.

3. Results and discussions

3.1. Effect of specimen thickness

A representative image of a free standing double notched tensile specimen is displayed in Fig. 1(a). The total width, w_t , and gauge length, L , of each specimen is 300 nm and 1700 nm, respectively. In these tests, the notch height, r , and the notch depth, d , as illustrated in Fig. 1(b), are both 75 nm, and the un-notched ligament length, w_u , is 150 nm for every specimen. Only the specimen thickness t was varied from 200 nm to 400 nm. The schematic illustration and the *in situ* TEM image of the specimen-grip assembly is provided in Tian et al. [28,29]. The nominal stress, σ_n , is measured as the ratio of applied load and the initial cross section of the ligament that connects the notches, whereas the nominal strain, ϵ_n , is measured as the change in gauge length, ΔL , divided by L . Fig. 2(a) displays the representative stress-strain curves from tensile tests on the notched specimens (individual curves have been shifted relative to each other). Irrespective of the specimen thickness, the stress-strain curves are characterized by an approximately linear elastic portion, up to $\epsilon_n \sim 4.5$ –5%, followed by fracture.

Un-notched MG specimens with similar dimensions also exhibit a similar stress-strain response under uniaxial tension [28,29]. A higher strain to failure, $\epsilon_f \sim 4$ –5% in submicron sized specimens, compared to $\epsilon_f \sim 2\%$ in bulk MGs, is a consequence of the former's smaller volume. Smaller volumes delay the onset of catastrophic failure because an embryonic SB (formed from activated STZs) is geometrically confined, thus preventing it from maturing into a macroscopic SB [28,30]. This allows locally stronger regions in the structurally heterogeneous MG to deform elastically even after the strain exceeds 2%.

It was also observed that the peak nominal stress, σ_s , of 200 and 300 nm thick specimens are comparable, and are as high as $\sim 3.92 \pm 0.14$ GPa (See Fig. 2(a)). However, when t is increased to 350 nm and 400 nm, σ_s reduces to $\sim 3.72 \pm 0.17$ GPa. Previous studies show that the strength of unnotched specimens with similar dimensions is also in the range of 3.5–3.9 GPa [28]. Therefore, the relative invariance in ϵ_f and σ_s , regardless of whether the specimen contains notches, tentatively suggests that the mechanical properties of submicron scale MGs are notch insensitive.

Next, we examined the fractured specimens to see if the mode of failure is also insensitive to the presence of notches. In unnotched tensile specimens, fracture occurs when a dominant SB nucleates at some surface undulation and propagates along a plane oriented at an angle, $\theta \sim 55$ –60°, to the loading axis [26,29]. While notched specimens with $t \geq 350$ nm appear to fail in the same manner as unnotched specimens, i.e. fracture occurs along a plane inclined at some angle to the loading axis (See Fig. 2(b) and Video S1a), the fractured side profiles of thinner specimens ($t \leq 300$ nm) are perpendicular to the loading axis (See Fig. 2(c) and Video S1b).

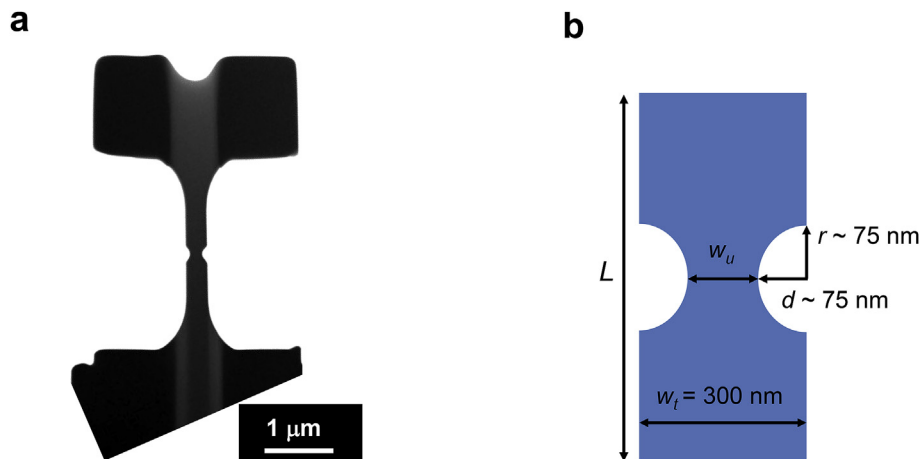


Fig. 1. Experimental set up for tensile tests on notched specimens. (a) Representative TEM image of a notch tensile specimen. (b) Cartoon depicting the different dimensions of the specimen.

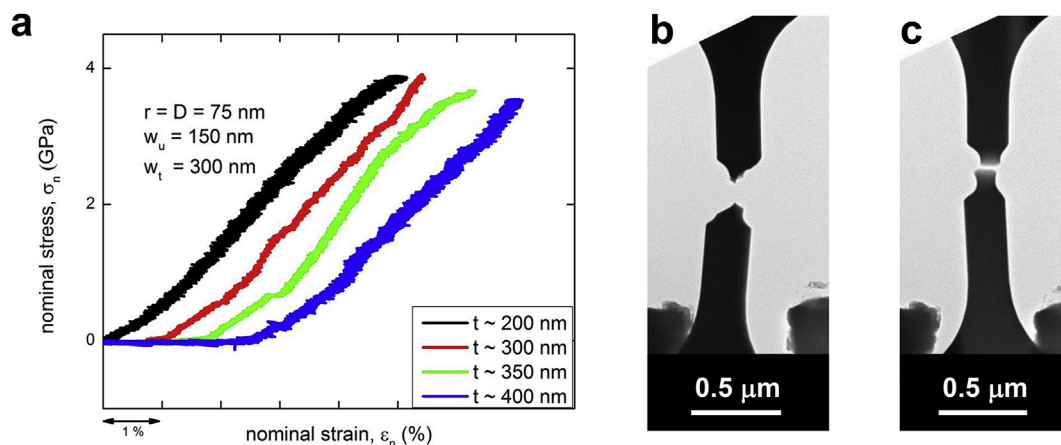


Fig. 2. Tensile tests on shallow notched specimens with different thickness. (a) Representation of nominal stress-strain curves for specimens with different t at a strain rate = $1 \cdot 10^{-3} \text{ s}^{-1}$. Curves have been shifted relative to each other for the sake of clarity. TEM images of the side profile of notch specimens with (b) $t \sim 350 \text{ nm}$ and (c) $t \sim 200 \text{ nm}$, respectively, after fracture.

Clearly, there is a change in the mode of failure when the specimen thickness changes, although in both cases, failure always occurs within the ligament that connects the notches.

Supplementary video related to this article can be found at <https://doi.org/10.1016/j.actamat.2018.05.041>.

To understand this transition, it is important to first examine the mechanism of fracture in MGs. Irrespective of the specimen thickness, when a notched MG specimen is loaded, SBs nucleate ahead of each notch tip, along trajectories described by Prandtl and logarithmic spiral slip-line fields [31,32]. Tandaiya et al. suggested that amongst these SBs, an incipient crack prefers to grow inside the SB oriented in the direction of the maximum plastic strain. From simulations, it was determined that the trajectory with the maximum plastic strain is oriented at an angle of $\theta = \pm 69^\circ$ from the notch line [33,34]. Due to symmetry, SBs propagating from both notches intersect and precipitate failure. Now, the plane along which the surfaces separate, during fracture, depends on the dimensions of the specimen. In thinner specimens ($t < 300$), a plane stress condition prevails due to the absence of constraint in the thickness direction. Under this condition, failure is characterized by the specimen surfaces separating in the out-of-plane (thickness) direction, along an angle θ with the loading axis (See Fig. S1 in supplementary information (SI) for more details). Alternately,

when the specimen is sufficiently thick (See Fig. S2 in SI), it undergoes failure in constrained plane strain mode and the surfaces separate in the width direction along some other plane inclined to the loading axis. Both these modes of failure are illustrated in Fig. 3(a) and (b), respectively. This particular transition in failure modes, with changing thickness, has also been previously noted by Kimura and Masumoto in notched bulk MG specimens [17].

To understand the basis for this transition, we derived a simplified, first order approximation of the plastic work done during fracture in both these modes. Consider that the fracture surfaces of the unnotched ligament (with width, w_u and thickness, t) separate by a distance, s , under the shear stress, τ along a plane of shear, oriented at θ with the loading axis, as illustrated in Fig. 3(c). The work done on separating the surfaces along t under plane stress conditions, $W_{PI \text{ stress}}$, is

$$W_{PI \text{ stress}} = \int_0^{\frac{t}{\sin \theta}} \tau \cdot \left(\frac{t}{\sin \theta} - s \right) w_u \cdot ds \quad (1)$$

Assuming that the shear stress is constant and equal to the flow stress within the SB, on integrating Eq. (1) we get,

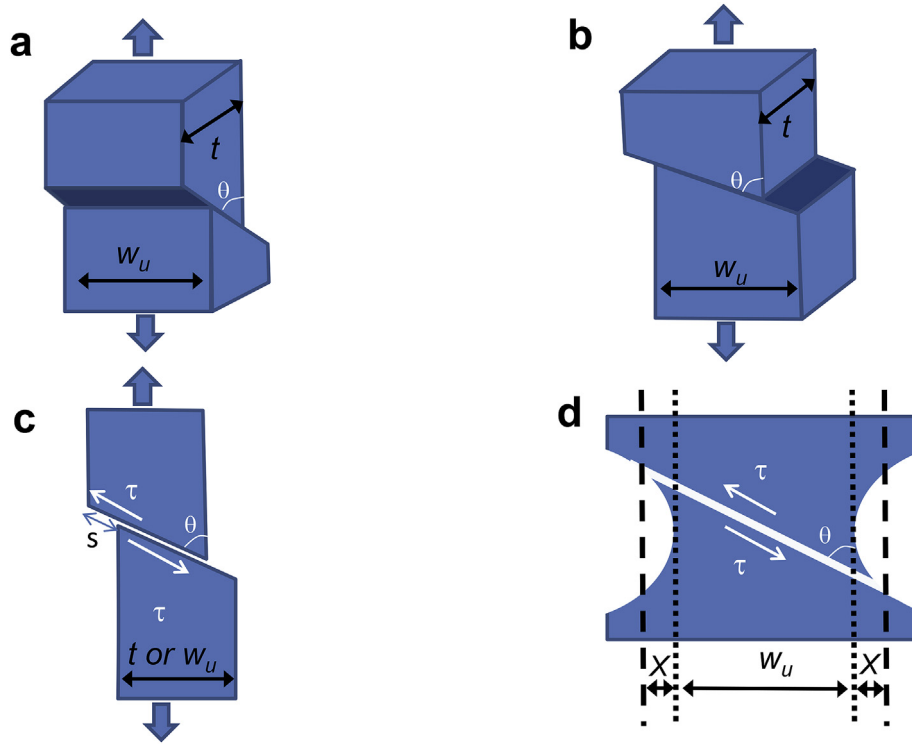


Fig. 3. Modes of failure for different specimen thicknesses. Illustrations of (a) plane stress mode of failure for $t < 300$ nm, (b) plane strain mode of failure for $t > 300$ nm, (c) a simplified model for failure for calculating the plastic work (d) effects of curvature and deviation of plane strain mode of failure from the model shown in (c).

$$WPI \text{ stress} = \frac{1}{2} \tau \cdot w_u \left(\frac{t}{\sin\theta} \right)^2 \quad (2)$$

Similarly, if the specimen fails along the w_u , the total plastic work done under plane strain conditions, $W_{Pl \text{ strain}}$, can be written as

$$WPI \text{ stress} = \int_0^{\frac{w_u}{\sin\theta}} \tau \cdot \left(\frac{w_u}{\sin\theta} - s \right) t \cdot ds \quad (3)$$

Before integrating Eq. (3), a subtle difference between failure in the plane stress and plane strain mode needs to be considered. The general shape of the failing section in our simplified model, which corresponds to the ligament that connects the notches, has been approximated as a parallelepiped (see Fig. 3(a) and (b)). Such an approximation works for the plane stress mode as it accurately models the ligament failure in the out-of- plane direction. However, since the same approximation ignores the curvatures introduced by notches on the in-plane vertical edges of the section, the integration pathway for failure in the plane strain mode is inaccurate. A schematic illustration of the actual ligament, failing in the plane strain mode is displayed in Fig. 3(d). The region bounded by the two dotted vertical lines, with width w_u and whose work of failure is described by Eq. (3), corresponds to the part of the ligament modelled in Fig. 3(c). However, since fracture occurs at an angle, certain portions of the ligament, with widths X , also lie beyond this bounded region. Note that the work of failure of these portions have not been considered while formulating Eq. (3). Hence, the actual work of failure in plane strain will be higher than what is calculated from the model. To adjust for this difference, an empirical factor, α , is multiplied to $W_{Pl \text{ strain}}$ in Eq. (3) after integration and is now written as,

$$WPI \text{ stress} = \frac{1}{2} \alpha \tau \cdot t \left(\frac{w_u}{\sin\theta} \right)^2 \quad (4)$$

Comparing eqs. (2) and (4) we get the ratio of the total plastic work done under plane strain conditions, $W_{Pl \text{ strain}}$, and the work done under plane stress conditions,

$$\frac{W_{Pl \text{ strain}}}{W_{Pl \text{ stress}}} = \frac{\alpha w_u}{t} \quad (5)$$

Overall, this derivation is based on the assumption that the top half of the specimen slides over the bottom half either along t or w_u . In such a scenario, beyond the peak load, the load should drop linearly from peak value to zero with an attendant increase in the load point displacement by $t/\tan\theta$ or $w_u/\tan\theta$. Since the post peak portion of the stress-strain curves for each specimen in Fig. 2(a) have been removed for aesthetic purposes, it appears that the load abruptly drops to zero. However, a representative load-displacement curve in Fig. S2a shows that the post peak displacement indeed increases for all specimens, which validates the use of the above-developed model. Additional evidence for sliding of the two fracture surfaces over each other can be seen in Fig. S2b and Video S1a.

From Eq. (5) it is clear that, for a fixed value of w_u (~150 nm), the transition in the mode of failure from plane stress to plane strain, which occurs when $W_{Pl \text{ strain}} = W_{Pl \text{ stress}}$, depends on t and α . Our experiments show that this transition occurs when $300 \text{ nm} < t < 350 \text{ nm}$, implying that $\alpha \approx 2$. It appears that failure of the exterior portions of the ligament, which are excluded from our simplified model, contribute to about 50% of $W_{Pl \text{ strain}}$. Such a high proportion of contribution to $W_{Pl \text{ strain}}$ from ligament portions whose net widths are much smaller than w_u is not unusual. This is because, although the integration paths of these portions are smaller, the work done in fracturing them can reach high values as

the value of τ near the notch roots are at least twice as high as that in the rest of the ligament. There are other factors that may affect the exact value of α but have not been considered in the preceding analysis. Some of these factors pertain to the broad assumptions made while deriving Eq. (5), which are as follows.

First, the cross section of the ligament was assumed to be uniform in the calculations (see Fig. 3(a) and (b)). Therefore, the state of stress, within the ligament, is also implicitly assumed to be uniform. However, this is only an approximation because in reality, the finite curvature of notches introduces stress concentrations and gradients in the material, which implies that τ no longer remains constant, but will also vary as a function of s . Second, the degree of stress triaxiality in the ligament that connects the notches progressively increases with increasing specimen thickness. Therefore, although we assumed that the value of τ in eqns. (2) and (4) is the same, they might actually be different. Third, the material inside a SB nucleus becomes soft and liquid-like and is often associated with temperature excursions. However, we have not considered temperature rise and frictional effects that can arise due to sliding in our derivations. Finally, it was assumed that the fracture plane, in both modes of failure, although separating in different directions, is always oriented at θ w.r.t. the loading axis. However, this aspect could not be confirmed as it was quite difficult to determine the exact angle made by the fracture plane, with the loading axis in the plane stress failure mode.

Even though a more rigorous analysis would lead to slightly different but more accurate equations for the works of failure in the two modes, we believe that their ratios would be very similar in spirit – at least in terms of the dependence on w_u and t – to that derived in Eq. (5).

While the preceding analysis establishes that changes in specimen thickness can significantly influence the mode of failure, it is interesting that the strength is relatively unaffected by it. Note that for all specimens, including unnotched ones, the deformation mechanism is primarily controlled by the dynamics of nucleating and propagating SBs. Therefore, the effectiveness in confining SBs decides the strength of submicron sized MGs specimens. To elaborate, notches constrain plasticity [18], which, by extension, should confine SBs to a greater degree. However, it is possible that, at the nanoscale, the constraint achieved with the hitherto employed notch dimensions may not be significant enough to add to the confining effects of the specimen volume. This argument is also consistent with the observation that notched specimens with $t \leq 300$ nm have the highest nominal strength ($\sigma_s \sim 3.92$ GPa), even though they have the same notch dimensions as thicker specimens.

3.2. Effect of notch sharpness

To examine whether modifying the notch dimensions can result in different constraint levels we adjusted the notch aspect ratio in thicker specimens ($t \geq 350$ nm). Free standing tensile specimens with sharp notches were fabricated as shown in Fig. 4(a).

Owing to limitations of the FIB setup, the smallest achievable r , with $t \sim 350$ nm, is 20 nm (See the illustration in Fig. 4(b)). The nominal stress-strain response of specimens with $w_u \sim 150$ nm and $r \sim 75$ nm and 20 nm, on being loaded in tension, is shown in Fig. 5. Like the specimens with shallower notches (see Fig. 2(a) and Videos S1a and S1b), these specimens also display a steady approximately linear elastic response until $\epsilon_n \sim 5\%$ and then fail catastrophically (See Video S2). However, note that for the same $w_u \sim 150$ nm, $\sigma_s \sim 4.16 \pm 0.09$ GPa for a notch with $r \sim 20$ nm, while $\sigma_s \sim 3.62 \pm 0.07$ GPa for $r \sim 75$ nm. An increase in nominal strength, purely facilitated by the change in notch shape, suggests that the geometry of the notch influences the stress state in the ligament connecting the notches (The 14% increase in nominal strength is

beyond acceptable scatter bounds and thus statistically significant). To describe the stress state within the ligament, the stress triaxiality, η , for plane strain flat notch specimens is derived from the Bridgeman analysis of necking and is mathematically represented as [35]:

$$\eta = \frac{\sigma_m}{\sigma_{eq}} = \frac{\sqrt{3}}{3} \left[1 + 2 \ln \left[1 + \frac{w_u}{4r} \right] \right] \quad (6)$$

where the ratio of the width of the ligament between the notches and the notch root radius (w_u/r) is designated as the notch sharpness¹; σ_m and σ_{eq} are the hydrostatic stress and von Mises equivalent stress, respectively. Note that the stress triaxiality, which denotes the balance between hydrostatic and deviatoric stresses, quantitatively describes the competition between void formation and SB nucleation [7]. In Fig. 6(a), the variations in η are plotted as a function of notch sharpness. As a reference, the data points corresponding to specimens employed in this study have been highlighted in the figure. For a notch free tensile specimen ($r \sim \infty$), the logarithmic term equals zero and $\eta = 1/\sqrt{3}$. With increasing notch sharpness (or decreasing r), the stress triaxiality in the ligament connecting the notches also increases. For the specimens tested in the present study, the value of η increases to 1.303 from a modest value of 1.04, when r is reduced from 75 nm to 20 nm. Since a high degree of triaxiality will mitigate the nucleation of SBs, specimens with sharp notches ($r \sim 20$ nm) will yield at higher stresses compared to the ones with blunt notches ($r \sim 75$ nm).

In some circumstances, when the value of η exceeds a certain threshold, the deformation mechanism transitions from shear localization to void nucleation and coalescence. This threshold value, characterized by the ratio of cavitation stress to the shear localization stress, σ_c/σ_s , is dependent on the composition of the material and is also highly sensitive to flaws. After conducting MD simulations on a model Cu₅₀Zr₅₀ MG, the critical value of σ_c/σ_s was determined to be 2.6 [19]. Therefore, whenever $\eta \geq 2.6$ (marked with a horizontal line in Fig. 6(a)), fracture will be mediated by the growth and coalescence of cavities. Since $\eta \leq 2.6$ for all the specimens employed in the present study, failure occurs via strain localization within nucleated SBs. Evidence of SB mediated fracture can be seen in Fig. 6(b), where the surface of a fractured specimen is inclined at $\theta \sim 45^\circ$ to the loading direction (cavitation would result in fracture surfaces that are inclined at $\theta \sim 90^\circ$ to the loading axis). Alternatively, cavitation could be precipitated by employing sharper notches ($r < 20$ nm) or by designing specimens with greater widths ($w_u > 400$ nm; $r \sim 20$ nm). Attempts to prepare specimens with sharper notches proved futile but we believe that future advancements in specimen preparations may validate the above-mentioned transition in deformation mechanisms. Similarly, although it is possible to develop specimens with $w_u > 400$ nm, our load cell's inability to sustain large loads prevents us from performing these tests.

It is however noteworthy that an increase in nominal strength, as a function of increased notch sharpness, has also been observed in bulk MG specimens [19]. Unlike the results of the present study, where a strength increment of only 14% is observed, Pan et al. [19] recorded a 2 fold increase in strength with increasing notch sharpness. The reason for such contrasting degrees of enhancement in strengths for bulk and sub-micron scale notched specimens is

¹ In a cylindrical specimen with a circumferential notch, notch sharpness is uniquely defined in terms of the ratio of the diameter of the ligament and the notch root radius, d/r . However, for double notched plate specimens, w_u/r , is used instead. This modified equation was derived and verified with complementary finite element simulations and experiments by Bai et al. [35].

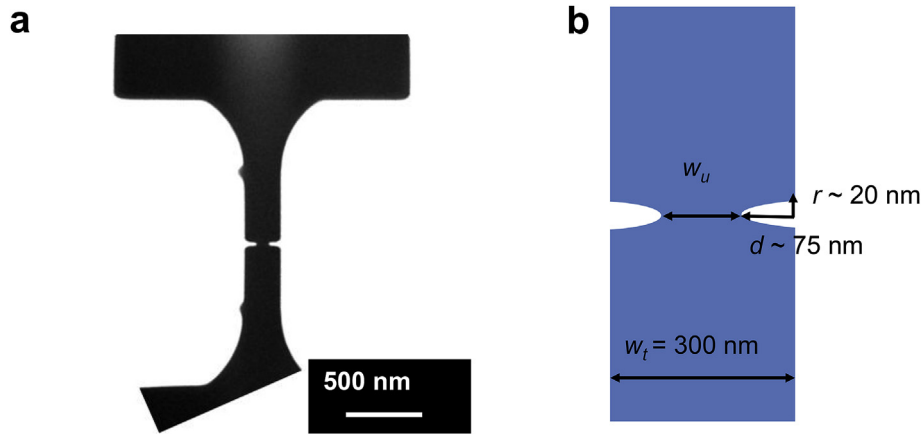


Fig. 4. Experimental set up for tensile tests on specimens with sharp notches. (a) Representative TEM image of a sharp notched tensile specimen. (b) Cartoon depicting the different dimensions of the specimen.

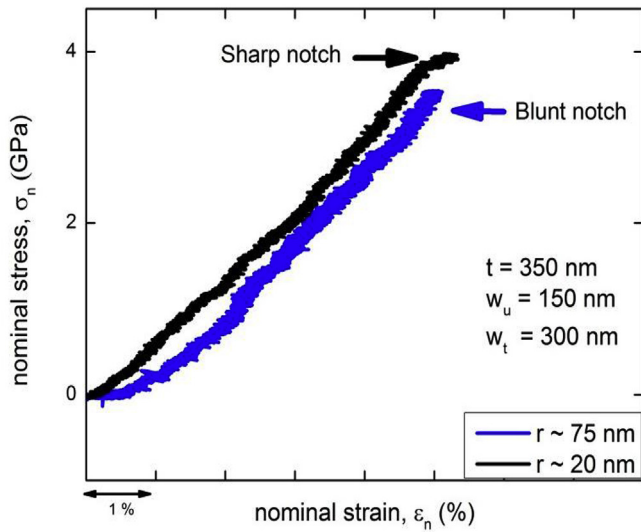


Fig. 5. Tensile tests on sharp notch specimens. Representative nominal stress-strain curves for specimens with different notch root radius, r . Curves have been shifted relative to each other for the sake of clarity.

the following. In bulk MGs, the assured presence of flaws and stress raisers within its volume promotes easy nucleation of SBs. Therefore, the strength of bulk MGs is comparatively low (~2 GPa) and any enhancement in strength can only be achieved by mitigating the growth of SBs. Notches, by the virtue of introducing a stress gradient, mitigate the growth of SBs and lead to a modest increase in the strength. For instance, Qu et al. [21] reported that bulk MG, with relatively blunt notches, are only a 1.14 times stronger than their unnotched counterparts. However, Pan et al. employed an extremely sharp notch, which severely constrains plastic flow; to an extent that SB formation is altogether suppressed and cavitation induced failure occurs. This complete suppression of shear mediated plastic flow, in addition to the operation of a high stress cavitation process, enhances the strength dramatically in bulk specimens. In contrast, as mentioned earlier, in submicron MG specimens, even in the absence of notches, SB nucleation is limited by the reduced dimensions and absence of flaws. Therefore, although the presence of notches assists in mitigating SB nucleation, it is only marginally adds to the geometrical confinement effect. Hence unless transition to cavitation induced failure occurs, the limited strength elevation in sub-micron scale specimens with increased notch sharpness is justified.

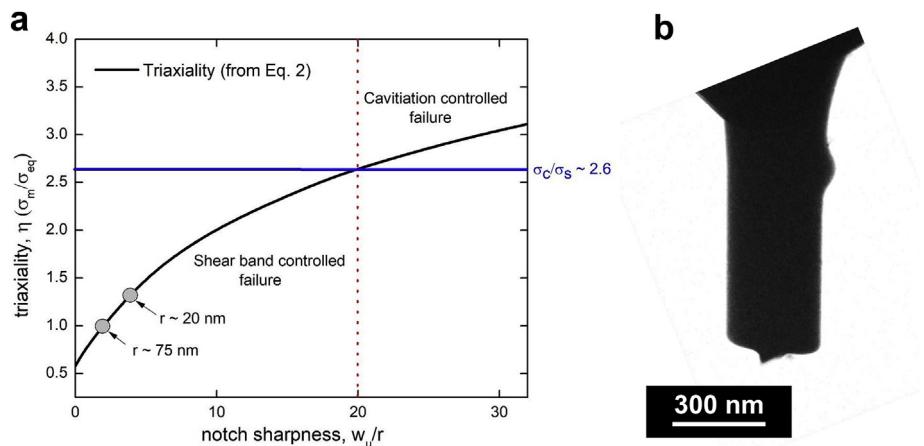


Fig. 6. The effect of stress triaxiality as a function of notch sharpness (a) Variation of triaxiality with w_u/r . When $\eta \geq \sigma_c/\sigma_s$ (indicated by horizontal blue line), transition from shear banding to void growth occurs. Note that w_u/r equals zero in a notch-free specimen. (b) TEM images of the side profile of sharp notch specimen after fracture. Fracture roughly occurs at an angle $\theta \sim 55^\circ$, implying that failure is mediated by a shear band and not by cavitation. (For interpretation of the references to colour in this figure legend, the reader is referred to the Web version of this article.)

3.3. Effect of notch depth

Next, we investigate the influence of deeper notches on the strength and deformation response of submicron sized MGs specimens. While fixing $t \sim 350$ nm and $r \sim 20$ nm, specimens with w_u of 77 nm, 80 nm, 95 nm, 100 nm and 150 nm are designed. Their representative nominal stress-strain responses, on being loaded in tension, are displayed in Fig. 7.

The lack of macroscopic plasticity remains a recurring theme even in these specimens (also see Videos S3a and S3b). For specimens with w_u ranging between 150 nm and 95 nm, σ_s remains invariant and lies in the range ~ 3.95 – 4.12 GPa (see Fig. 7). However, when w_u is ~ 77 and 80 nm, σ_s drops to ~ 2.62 and 3.05 GPa. It is not clear if nominal strength would further drop if w_u is reduced because it was impossible to mill deeper notches in free standing specimens using the present FIB setup. Alternatively, we were able to make deeper notches in push-to-pull (PTP) tensile specimens. The image and schematic of one such specimen is shown in Fig. 8(a) and (b), and the details of how it was designed is provided elsewhere [36]. Dimensions t and r were maintained as 350 nm and 20 nm respectively, whereas $w_t \sim 500$ nm and $L \sim 1000$ nm (see Fig. 8(c)). The strain rate employed for free standing specimens is maintained by adjusting the loading rate accordingly. It was determined that the specimen predominantly experiences tensile displacements in the entire duration of the test (see Fig. S4 in SI). The main disadvantage of this setup is that the load borne by the tensile specimen cannot be measured. Therefore, although the changes in σ_s cannot be measured, any other qualitative changes associated with smaller ligaments that connect the notches can be captured with this setup. To compare the qualitative aspects of deformation in PTP and free standing tensile specimens, we first tested a specimen with $w_u \sim 80$ nm. Just like the free-standing specimens hitherto tested, the PTP specimens also fail within the ligament that connects the notches in a brittle fashion with two SBs intersecting at the notch tip (See Video S4 and Fig. 8(d)). However, when a PTP specimen with $w_u \sim 60$ nm is pulled in tension, the ligament that connects the notches exhibits ductility before failing by necking to a point (See Video S5).

Utilizing a series of snapshots captured from the video, we will chronologically describe the events occurring during the test. Fig. 9(a) shows an image of the specimen in the unstressed state. When the strain in the ligament reaches $\sim 5\%$, the edges of ligament

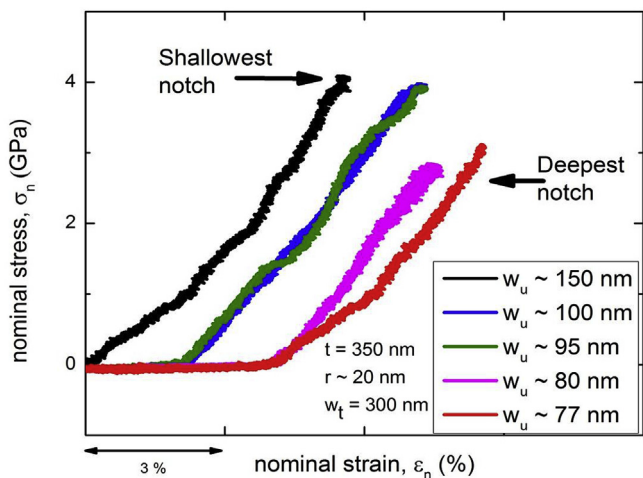


Fig. 7. Tensile tests on sharp notch specimens with different notch ligament widths. nominal stress-strain curves for specimens with different widths of ligament between notches, w_u . Curves have been shifted relative to each other for the sake of clarity.

that connects the notches start thinning (see Fig. 9(b)). On further straining, an incipient elliptical band (marked by red arrows) resembling a SB nucleus forms at the notch edges and spreads into the ligament that connects the notches (see Fig. 9(c)). Note that the size of this elliptical band is slightly lesser in one edge compared to the other. For perfectly symmetric notches, the growth of SB nuclei should also be symmetric. However, despite our best efforts, minor dimensional differences between the two notches (or surface irregularities) can result in slightly different SB nuclei sizes. Once this happens, the larger SB nuclei would grow at the expense of the other, owing to the intrinsic strain softening nature of the material. Finally, necking occurs when the elliptical bands from both notches merge together, within the ligament (See Fig. 9(d) and (e)).

Up until now, the brittle-to-ductile transition (BDT) in notched MG specimens has only been predicted by MD and FEA simulations. Unlike in crystalline materials where the BDT is the result of competition between cleavage fracture (brittle) and dislocation activities (ductile) [37–39], the competing mechanisms of BDT in MGs are SB-induced failure (brittle) and homogeneous activation of STZs (ductile). To explain this transition, various mechanisms, ranging from SB interactions to the geometric inability to sustain a SB nucleus, have been offered in literature [23,24,40]. Deriving a few key features from different constitutive models, a simplified and qualitative explanation of the BDT in this study is as follows. Notches in any material introduce a stress and strain gradient ahead of them. Therefore, although the stresses and strains close to the notch root are high enough to activate STZs and form an embryonic SB, the rest of the ligament that connects the notches experiences only elastic stresses and strains. This also generates a free volume gradient ahead of the embryonic SB tip. Free volume is a thermodynamic entity, which describes the local packing efficiency of a MG [41]. In the context of deformation mechanisms, a higher free volume content assists in activating more STZs [42,43]. Also, since its content is directly related to interatomic stretching, highly stressed regions tend to accumulate more free volume [18,42]. The stresses arising due to the gradient in free volume has also been interpreted in the form of a parameter known as the interaction stress, μ [44,45]. Typically, if $\mu < 0$, plastic straining is promoted, whereas it is prevented if $\mu > 0$. Since μ directly scales with free volume content, an intrinsic material length scale, l_c , which measures the distance up to which $\mu > 0$, is introduced to characterize deformation in MGs [25]. This has the following implications on the shear banding. A larger value of l_c implies that μ will be positive over longer lengths or an incipient SB will grow stably and involve more defects, which in turn, homogenizes deformation. Typically, alloys having larger l_c would have a composition that promotes profuse activation of STZs.

In notched specimens, when a SB forms inside the plastic zones in front of the notch tips, the free volume content increases and $\mu > 0$ within the SB. On the other hand, $\mu < 0$ at the outer edges of the shear band, which tends to widen the SB [24]. The relative balance and locations of the of positive and negative μ will determine whether the plastic zones will expand within the ligament or facilitate early shear localization within SBs. For instance, Dutta et al. [25] showed that when blunt notches are employed the stress concentration at the notch tip will be low. A low stress concentration implies that μ will be lower and more uniformly distributed at the notch root which can then be effectively counterbalanced by negative pockets of μ . This leads to growth of the notch tip plastic zones and widening of SBs. Alternately, in the presence of sharp notches, the stress concentration is very high and the steep increase of μ inside SBs is not counterbalanced by negative μ at the SB edges. Therefore, plastic zones cannot advance further inside the ligament and failure occurs via rapid strain localization along SBs. The limited growth of plastic zones due to the imbalance in

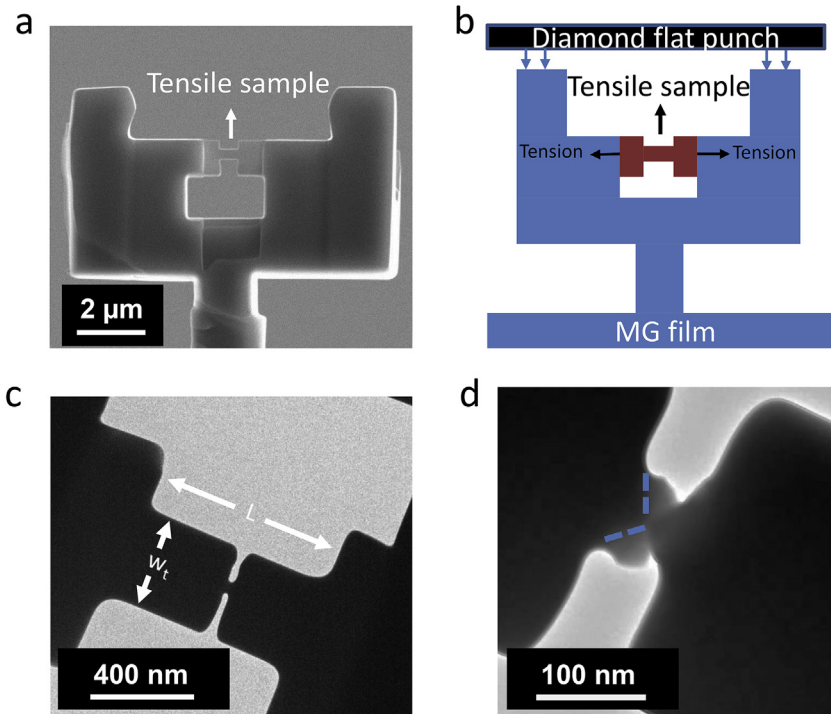


Fig. 8. Tension tests on the push-to-pull (PTP) sample. (a) SEM image of a tensile specimen fabricated by FIB, before milling in notches. (b) Schematic illustration of the setup. (c) Zoomed in TEM image of the notched tensile specimen with $w_u \sim 80$ nm. (d) TEM image of the side profile of the specimen in (c) after fracture.

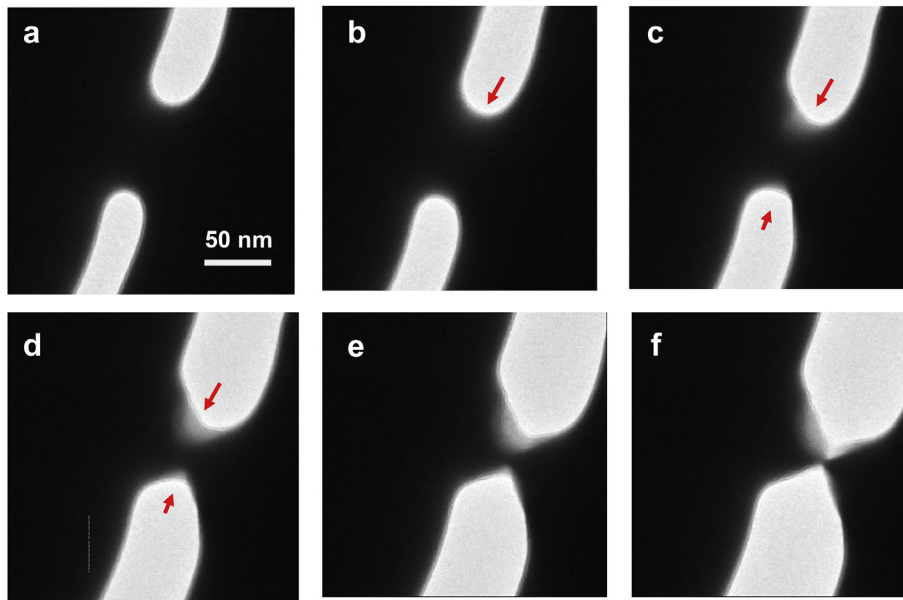


Fig. 9. Necking observed during the tensile test of a sample with $w_u = 60$ nm. (a–f) Snapshots extracted from the recorded movie inside the TEM. The red arrows indicate the locations of the growing incipient elliptical bands at the notch edges. (For interpretation of the references to colour in this figure legend, the reader is referred to the Web version of this article.)

interaction stresses explains why specimens with $r \sim 20$ nm and $w_u > 80$ nm in our study fail by SB propagation. However, if the value of w_u is sufficiently lowered, even the small plastic zones at either notch tip can overlap, mitigate strain localization within the two SB nuclei and lead to net yielding of the ligament. We believe that this overlap between plastic zones occurs in our PTP specimens with $w_u \sim 60$ nm, because of which, the ligament between the notches undergoes necking to a point despite the formation of SB

nuclei at the notch tips.

The competition between shear localization within SBs and homogeneous deformation mediated by overlapping of plastic zones may reach a tipping point when $w_u \sim 70$ – 80 nm. When this happens, the plastic zones from opposing notch tips will only overlap partially, leading to the interruption of shear localization by homogeneous flow and subsequent ligament yielding (the same is observed in one of the PTP specimens with $w_u \sim 75$ nm in Video S6).

The onset of homogeneous deformation in these specimens also coincides with the reduction in their nominal strength. A similar reduction in tensile strength was observed by Tian et al. [29] when specimens with dimensions, t , $w_t \sim 80$ nm, deformed homogeneously and exhibited necking.

However, a $Zr_{35}Ti_{30}Co_6Be_{29}$ MG of similar dimensions pulled in tension exhibits higher yield strength and undergoes strain hardening in the homogenous deformation regime [46]. The underlying origin of this discrepancy in deformation behavior for the two compositions is probably related to the material length scale l_c . Although its exact behavior at the microscopic level is not very clear at the moment, the value of l_c , which is a function of the free volume distribution and STZ character, may be much lower in $Cu_{49}Zr_{51}$ than that in $Zr_{35}Ti_{30}Co_6Be_{29}$. This would imply that SBs in the former are much narrower and are more susceptible to strain localization-induced failure than in the latter. There is additional evidence to support the possibility that l_c in $Cu_{49}Zr_{51}$ MG is low. For specimens with a notch acuity, $2r/w_u \sim 1$, Dutta et al. [25] suggest that the deformation behavior transitions from ligament necking to SB propagation when the value of l_c/w_u is low. Note that the above-mentioned notch geometry and specimen dimensions are identical to that of our blunt notch specimens ($r \sim 75$ nm and $w_u \sim 150$ nm) that failed by SB propagation. While this partially validates our hypothesis that $Cu_{49}Zr_{51}$ MGs have a low value of l_c , there is a case for conducting additional experimental investigations on specimens with higher $2r/w_u$. With the current setup, however, it is difficult to prepare and test specimens with $w_u < 100$ nm.

From the preceding discussions, it is evident that μ and l_c play a significant role in determining the BDT transition in notched MG specimens. While the latter is a function of MG composition and its thermal history, the former depends on the notch acuity of the specimens. Further dedicated experimental studies on different composition and varying notch dimensions can help in a comprehensive assessment of the theoretical models hitherto developed. Moreover, our future efforts will be directed towards testing specimens using a newly developed PTP setup by Bauer et al. [47] that can provide a quantitative estimate of the nominal strength of acutely notched specimens. Nevertheless, the present study is a first of a kind experimental investigation on the effects of specimen and notch geometry on the deformation response of MGs.

4. Summary and conclusions

By conducting real time *in situ* TEM tensile tests on notched submicron scale specimens, we studied the different aspects of notch sensitivity in MGs. It was found that the strength of MGs indeed displays varying degrees of notch sensitivities with changes in certain dimensions. While changing the specimen thickness only mildly affects the nominal strength of the MG, it alters the mode of failure. However, changes in notch sharpness and notch depth have significant yet contrasting effects on the strength of MGs. This is due to the different roles played by notch dimensions in constraining SB activity. Sharper notches promote material strengthening, as higher stress triaxiality reduces the resolved shear stress in the ligament, which then delays the nucleation of SBs. On the other hand, in the presence of deeper notches, can lead to overlap of plastic zones that promotes homogeneous deformation of the ligament. Depending on the composition and the internal state of the MG homogeneous deformation can result in reduction or enhancement in strength. Previous experimental studies have not been able to identify most of these subtle transitions due to several reasons. Gu et al. [26] were unable to report the nominal strength of notched tensile MG specimens because their notch dimensions were indeterminable. Only some simulation studies, which relied on FEM [24,25] and MD [23] simulations, have partially predicted

some aspects of notch sensitivity and also alluded to the existence of a brittle to ductile transition below a certain length scale. Combining these theoretical investigations with the experimental observations in this study, the transition was found to depend on two parameters, a) an intrinsic material parameter that is related to the distribution of free volume, and b) the notch geometry or specifically its acuity, which is defined as $2r/w_u$. It should also be mentioned that higher levels of strengthening was reported for circumferentially notched bulk MG specimens, compared to that of the double notched plate specimens [17,19]. Although investigating this particular aspect remains outside the scope of the current study, we believe that circumferential notches might also potentially offer higher levels of plastic constraint, and hence higher strengthening, at the submicron level.

In conclusion, our results show that intelligent design, which involves optimizing the thickness and controlling the aspect ratios of changes in cross sections and kinks, can enhance the endurance and performance of submicron and nano scale components made with MGs.

Acknowledgements

RLN and KJH are partially supported by Carnegie Mellon University. LT acknowledges Natural Science Foundation of China (Grant 51501144), China Postdoctoral Science Foundation (2015M580842), and the Alexander von Humboldt foundation for financial support. The authors also wish to thank the reviewers for their extremely valuable comments, some of which went a long way in enhancing the quality of our manuscript. We would also like to thank Dr. Subra Suresh for helpful discussion on this work.

Appendix A. Supplementary data

Supplementary data related to this article can be found at <https://doi.org/10.1016/j.actamat.2018.05.041>.

References

- [1] C.A. Schuh, T.C. Hufnagel, U. Ramamurty, Mechanical behavior of amorphous alloys, *Acta Mater.* 55 (2007) 4067–4109, <https://doi.org/10.1016/j.actamat.2007.01.052>.
- [2] D.J. Magagnosc, W. Chen, G. Kumar, J. Schroers, D.S. Gianola, Thermo-mechanical behavior of molded metallic glass nanowires, *Sci. Rep.* 6 (2016), <https://doi.org/10.1038/srep19530>, 19530.
- [3] G. Kumar, A. Desai, J. Schroers, Bulk metallic glass: the smaller the better, *Adv. Mater.* 23 (2011) 461–476, <https://doi.org/10.1002/adma.201002148>.
- [4] H.M. Chiu, G. Kumar, J. Blawdziewicz, J. Schroers, Thermoplastic extrusion of bulk metallic glass, *Scripta Mater.* 61 (2009) 28–31, <https://doi.org/10.1016/j.scriptamat.2009.02.052>.
- [5] G. Duan, A. Wiest, M. Lind, J. Li, W.K. Rhim, W.L. Johnson, Bulk metallic glass with benchmark thermoplastic processability, *Adv. Mater.* 19 (2007) 4272–4275, <https://doi.org/10.1002/adma.200700969>.
- [6] J. Schroers, Q. Pham, A. Desai, Thermoplastic forming of bulk metallic glass—a technology for MEMS and microstructure fabrication, *J. Microelectromech. Syst.* 16 (2007), <https://doi.org/10.1109/JMEMS.0007.892889>.
- [7] R.W. Hertzberg, R.P. Vinci, J.L. Hertzberg, *Deformation and Fracture Mechanics of Engineering Materials*, John Wiley & Sons, Inc, 2012.
- [8] J. Rösler, H. Harders, M. Bäker, Mechanical behaviour of engineering materials metals, Ceramics, PolymCeram. Polym. Composers, and Composites (2007), <https://doi.org/10.1017/CBO9781107415324.004>.
- [9] T. Zhang, X. Li, S. Kadkhodaei, H. Gao, Flaw insensitive fracture in nanocrystalline graphene, *Nano Lett.* 12 (2012) 4605–4610, <https://doi.org/10.1021/nl301908b>.
- [10] H. Gao, B. Ji, I.L. Jager, E. Arzt, P. Fratzl, Materials become insensitive to flaws at nanoscale: lessons from nature, *Proc. Natl. Acad. Sci. U. S. A.* 100 (2003) 5597–5600, <https://doi.org/10.1073/pnas.0631609100>.
- [11] M.J. Buehler, H. Yao, H. Gao, B. Ji, Cracking and adhesion at small scales: atomistic and continuum studies of flaw tolerant nanostructures, *Model. Simulat. Mater. Sci. Eng.* 14 (2006) 799–816, <https://doi.org/10.1088/0965-0393/14/5/001>.
- [12] J.-Y. Kim, X. Gu, M. Wraith, J.T. Uhl, K. a. Dahmen, J.R. Greer, Suppression of catastrophic failure in metallic glass-polyisoprene nanolaminate containing nanopillars, *Adv. Funct. Mater.* 22 (2012) 1972–1980, <https://doi.org/10.1002/>

- adfm.201103050.
- [13] X.W. Gu, Z. Wu, Y.-W. Zhang, D.J. Srolovitz, J.R. Greer, Microstructure versus flaw: mechanisms of failure and strength in nanostructures, *Nano Lett.* 13 (2013) 5703–5709, <https://doi.org/10.1021/nl403453h>.
 - [14] A.R. Beaber, J.D. Nowak, O. Ugurlu, W.M. Mook, S.L. Girshick, R. Ballarini, W.W. Gerberich, Smaller is tougher, *Philos. Mag. A* 91 (2011) 7–9, <https://doi.org/10.1080/14786435.2010.487474>.
 - [15] M.D. Uchic, D.M. Dimiduk, J.N. Florando, W.D. Nix, Sample dimensions influence strength and crystal plasticity, *Science* 305 (2004) (80–), <http://science.sciencemag.org/content/305/5686/986.full>. (Accessed 26 May 2017).
 - [16] S. Kumar, X. Li, A. Haque, H. Gao, Is stress concentration relevant for nanocrystalline metals? *Nano Lett.* 11 (2011) 2510–2516, <https://doi.org/10.1021/nl201083t>.
 - [17] H. Kimura, T. Masumoto, Plastic constraint and ductility in tensile notched specimens of amorphous Pd78Cu6Si16, *Mater. Trans. A* 14 (1983) 709–716, <https://doi.org/10.1007/BF02643787>.
 - [18] Z.T. Wang, J. Pan, Y. Li, C. a Schuh, Densification and strain hardening of a metallic glass under tension at room temperature, *Phys. Rev. Lett.* 111 (2013), <https://doi.org/10.1103/PhysRevLett.111.135504>, 135504.
 - [19] J. Pan, H.F.F. Zhou, Z.T.T. Wang, Y. Li, H.J.J. Gao, Origin of anomalous inverse notch effect in bulk metallic glasses, *J. Mech. Phys. Solid.* 84 (2015) 85–94, <https://doi.org/10.1016/j.jmps.2015.07.006>.
 - [20] K. Flores, R. Dauskardt, Mean stress effects on flow localization and failure in a bulk metallic glass, *Acta Mater.* 49 (2001) 2527–2537. <http://www.sciencedirect.com/science/article/pii/S1359645401001252>. (Accessed 7 July 2014).
 - [21] R.T.T. Qu, M. Calin, J. Eckert, Z.F.F. Zhang, Metallic glasses: notch-insensitive materials, *Scripta Mater.* 66 (2012) 733–736, <https://doi.org/10.1016/j.scriptamat.2012.01.044>.
 - [22] R. Qu, P. Zhang, Z. Zhang, Notch effect of materials: strengthening or weakening? *J. Mater. Sci. Technol.* 30 (2014) 599–608, <https://doi.org/10.1016/j.jmst.2014.04.014>.
 - [23] Z.D. Sha, Q.X. Pei, Z.S. Liu, Y.W. Zhang, T.J. Wang, Necking and notch strengthening in metallic glass with symmetric sharp-and-deep notches, *Sci. Rep.* 5 (2015) 10797, <https://doi.org/10.1038/srep10797>.
 - [24] I. Singh, R. Narasimhan, Notch sensitivity in nanoscale metallic glass specimens: insights from continuum simulations, *J. Mech. Phys. Solid.* 86 (2016) 53–69, <https://doi.org/10.1016/j.jmps.2015.10.001>.
 - [25] T. Dutta, A. Chauniyal, I. Singh, R. Narasimhan, P. Thamburaja, U. Ramamurty, Plastic deformation and failure mechanisms in nano-scale notched metallic glass specimens under tensile loading, *J. Mech. Phys. Solid.* 111 (2018) 393–413, <https://doi.org/10.1016/j.jmps.2017.11.011>.
 - [26] X.W. Gu, M. Jafary-Zadeh, D.Z. Chen, Z. Wu, Y.W. Zhang, D.J. Srolovitz, J.R. Greer, Mechanisms of failure in nanoscale metallic glass, *Nano Lett.* 14 (2014) 5858–5864, <https://doi.org/10.1021/nl5027869>.
 - [27] A.S. Argon, Plastic deformation in metallic glasses, *Acta Metall.* 27 (1979) 47–58, [https://doi.org/10.1016/0001-6160\(79\)90055-5](https://doi.org/10.1016/0001-6160(79)90055-5).
 - [28] L. Tian, Y.-Q. Cheng, Z.-W. Shan, J. Li, C.-C. Wang, X.-D. Han, J. Sun, E. Ma, Approaching the ideal elastic limit of metallic glasses, *Nat. Commun.* 3 (2012) 609, <https://doi.org/10.1038/ncomms1619>.
 - [29] L. Tian, Z.-W.W. Shan, E. Ma, Ductile necking behavior of nanoscale metallic glasses under uniaxial tension at room temperature, *Acta Mater.* 61 (2013) 4823–4830, <https://doi.org/10.1016/j.actamat.2013.05.001>.
 - [30] F. Shimizu, S. Ogata, J. Li, Yield point of metallic glass, *Acta Mater.* 54 (2006) 4293–4298, <https://doi.org/10.1016/j.actamat.2006.05.024>.
 - [31] H. Kimura, T. Masumoto, Deformation and fracture of an amorphous Pd Cu Si alloy in V-notch bending tests—II: ductile–brittle transition, *Acta Metall.* 28 (1980) 1677–1693.
 - [32] K.M. Flores, R.H. Dauskardt, Crack-tip plasticity in bulk metallic glasses, *Mater. Sci. Eng. A* 319–321 (2001) 511–515, [https://doi.org/10.1016/S0921-5093\(01\)01111-X](https://doi.org/10.1016/S0921-5093(01)01111-X).
 - [33] P. Tandaiya, R. Narasimhan, U. Ramamurty, Mode I crack tip fields in amorphous materials with application to metallic glasses, *Acta Mater.* 55 (2007) 6541–6552, <https://doi.org/10.1016/j.actamat.2007.08.017>.
 - [34] P. Tandaiya, U. Ramamurty, R. Narasimhan, Mixed mode (I and II) crack tip fields in bulk metallic glasses, *J. Mech. Phys. Solid.* 57 (2009) 1880–1897, <https://doi.org/10.1016/j.jmps.2009.07.006>.
 - [35] Y. Bai, X. Teng, T. Wierzbicki, On the application of stress triaxiality formula for plane strain fracture testing, *J. Eng. Mater. Technol.* 131 (2009) 21002, <https://doi.org/10.1115/1.3078390>.
 - [36] M.-S. Ding, L. Tian, W.-Z. Han, J. Li, E. Ma, Z.-W. Shan, Nanobubble fragmentation and bubble-free-channel shear localization in Helium-irradiated sub-micron-sized copper, *Phys. Rev. Lett.* 117 (2016), <https://doi.org/10.1103/PhysRevLett.117.215501>, 215501.
 - [37] B.D. Ferney, K.J. Hsia, The influence of multiple slip systems on the brittle–ductile transition in silicon, *Mater. Sci. Eng. A* 272 (1999) 422–430, [https://doi.org/10.1016/S0921-5093\(99\)00514-6](https://doi.org/10.1016/S0921-5093(99)00514-6).
 - [38] Y.-B. Xin, K.J. Hsia, Simulation of the brittle–ductile transition in silicon single crystals using dislocation mechanics, *Acta Mater.* 45 (1997) 1747–1759, [https://doi.org/10.1016/S1359-6454\(96\)00274-1](https://doi.org/10.1016/S1359-6454(96)00274-1).
 - [39] K.J. Hsia, A.S. Argon, Experimental study of the mechanisms of brittle-to-ductile transition of cleavage fracture in Si single crystals, *Mater. Sci. Eng. A* (1994), [https://doi.org/10.1016/0921-5093\(94\)90964-4](https://doi.org/10.1016/0921-5093(94)90964-4).
 - [40] Q.K. Li, M. Li, Assessing the critical sizes for shear band formation in metallic glasses from molecular dynamics simulation, *Appl. Phys. Lett.* 91 (2007) 2005–2008, <https://doi.org/10.1063/1.2821832>.
 - [41] F. Spaepen, A microscopic mechanism for steady state inhomogeneous flow in metallic glasses, *Acta Metall.* 25 (1977) 407–415.
 - [42] L. Li, E.R. Homer, C.A. Schuh, Shear transformation zone dynamics model for metallic glasses incorporating free volume as a state variable, *Acta Mater.* 61 (2013) 3347–3359, <https://doi.org/10.1016/j.actamat.2013.02.024>.
 - [43] A.S. Argon, L.T. Shi, Development of visco-plastic deformation in metallic glasses, *Acta Metall.* 31 (1983) 499–507, [https://doi.org/10.1016/0001-6160\(83\)90038-X](https://doi.org/10.1016/0001-6160(83)90038-X).
 - [44] P. Thamburaja, R. Ekambaram, Coupled thermo-mechanical modelling of bulk-metallic glasses: theory, finite-element simulations and experimental verification, *J. Mech. Phys. Solid.* 55 (2007) 1236–1273, <https://doi.org/10.1016/j.jmps.2006.11.008>.
 - [45] P. Thamburaja, Length scale effects on the shear localization process in metallic glasses: a theoretical and computational study, *J. Mech. Phys. Solid.* 59 (2011) 1552–1575, <https://doi.org/10.1016/j.jmps.2011.04.018>.
 - [46] D. Jang, J.R. Greer, Transition from a strong-yet-brittle to a stronger-and-ductile state by size reduction of metallic glasses, *Nat. Mater.* 9 (2010) 215–219, <https://doi.org/10.1038/nmat2622>.
 - [47] J. Bauer, A. Schroer, R. Schwaiger, I. Tesari, C. Lange, L. Valdevit, O. Kraft, Push-to-pull tensile testing of ultra-strong nanoscale ceramic–polymer composites made by additive manufacturing, *Extrem. Mech. Lett.* 3 (2015) 105–112, <https://doi.org/10.1016/j.eml.2015.03.006>.